Thermal Analysis of a Skull Implant in Brain-Computer Interfaces

Claudia Serrano-Amenos[1], Frank Hu[2], Po T. Wang[1], Spencer Kellis[3], Richard A. Andersen[3], Charles Y. Liu[4], Payam Heydari[5], An H. Do[6], Zoran Nenadic[1,5]

***Abstract*— The goal of this study is to estimate the thermal impact of a titanium skull unit (SU) implanted on the exterior aspect of the human skull. We envision this unit to house the front-end of a fully implantable electrocorticogram (ECoG)-based bi-directional (BD) brain-computer interface (BCI). Starting from the bio-heat transfer equation with physiologically and anatomically constrained tissue parameters, we used the finite element method (FEM) implemented in COMSOL to build a computational model of the SU's thermal impact. Based on our simulations, we predicted that the SU could consume up to 75 mW of power without raising the temperature of surrounding tissues above the safe limits (increase in temperature of 1°C). This power budget by far exceeds the power consumption of our front-end prototypes, suggesting that this design can sustain the SU's ability to record ECoG signals and deliver cortical stimulation. These predictions will be used to further refine the existing SU design and inform the design of future SU prototypes.**

I. INTRODUCTION

Technological and medical advances are increasing the clinical adoption of active implantable devices. Examples include pacemakers, cochlear implants, and insulin pumps. Since these implants are electrically powered, they pose additional safety risks and must conform to the stringent Food and Drug Administration (FDA) safety requirements (ISO 14708-3). These include protection from inflammatory responses, electricity, and thermal injury. Thermal injury is caused by overheating of the surrounding tissues, which can lead to irreversible cell/tissue damage, including necrosis [1]. These risks are exacerbated for devices implanted in the head, such as cochlear implants [2], deep brain stimulators [3], and responsive neurostimulators (RNS) [4].

This study focuses on analyzing the thermal effect of a skull unit (SU) implant that is part of a fully-implantable brain-computer interface (BCI) system for the restoration of walking and leg sensation to people with paraplegia (see Fig. 1). Our group has been developing such a bi-directional (BD) BCI system for several years, including custom analog ultra-low-power (ULP) front-ends for recording [5], [6], [7], a low-power transceiver for wireless communication [8], and a benchtop prototype of the overall system [9]. We envision this system to record electrocorticogram (ECoG) signals from the leg motor cortex. These signals will be routed through the SU, where they will be amplified, serialized, and A/D converted. Subsequently, a tunneling cable will send them to a chest wall unit (CWU), where they will be analyzed and decoded. The CWU will also send wireless commands to an external end-effector (e.g., exoskeleton). It will also receive sensor data from the end-effector and convert them into stimulation patterns. These will, in turn, be sent via the tunneling cable to the SU, and delivered to the leg sensory cortex to elicit artificial sensation.

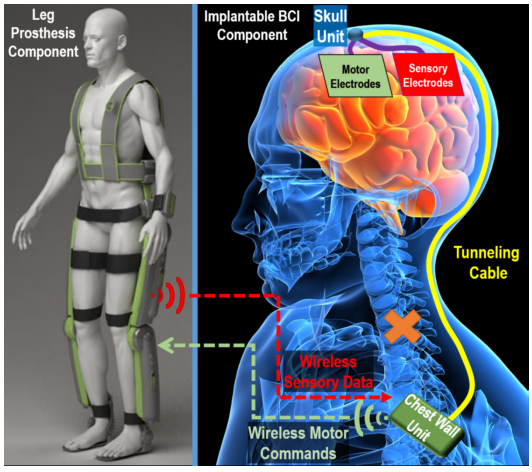

Fig. 1. Envisioned fully-implantable bi-directional BCI for the restoration of walking and leg sensation. The system comprises two implantable subsystems: the SU, implanted on the exterior aspect of the skull, and a chest wall unit (CWU), implanted subcutaneously in the pectoral area. The two subsystems are connected by a subcutaneous tunneling cable.

This study aims to predict the SU's power budget so that it can sustain the intended functions (amplification, serialization, A/D conversion) while conforming to the thermal safety requirements. Although establishing thermal safety ultimately requires *in vivo* testing, computational studies often represent the necessary first step to inform the design of the device and get a preliminary estimate of its thermal impact. Related studies have demonstrated the predictive value of bio-heat transfer models for deep brain stimulators [10], active intracortical microelectrode arrays [11], and fully-implantable intracortical BCIs [12]. However, the unique design of our SU and its implantation on the exterior aspect of the skull make it difficult to draw conclusions from these previous studies. Motivated by this knowledge gap, we

Work supported by the National Science Foundation (Award #1646275). C. Serrano-Amenos was partially supported by the Balsells Fellowship.

[1]Department of Biomedical Engineering, University of California Irvine (UCI), Irvine, CA 92697, USA {clauds3,znenadic}@uci.edu

[2]Department of Mechanical and Aerospace Engineering, UCI, Irvine, CA 92697, USA

[3]Division of Biology and Biological Engineering, CALTECH, Pasadena, CA 91125, USA

[4]Department of Neurological Surgery, University of Southern California, Los Angeles, CA 90033, USA

[5]Department of Electrical Engineering and Computer Science, UCI, Irvine, CA 92697, USA

[6]Department of Neurology, UCI, Irvine, CA 92697, USA

created a numerical model of the SU's thermal impact on neighboring tissues and estimated its power budget subject to FDA safety constraints. Our predictions will be used to refine the design of custom ULP integrated circuits for ECoG signal amplification, serialization, and A/D conversion.

II. MATERIALS AND METHODS

The thermal impact of the SU was modeled using Pennes' bio-heat equation with physiologically and anatomically constrained tissue parameters. The equations were solved using the finite element method (FEM) implemented in COMSOL Multiphysics (COMSOL, Inc.) software.

A. Geometric Model

The geometric model consisted of a cylindrical region (radius = 5 cm, height $\approx$ 6.5 cm) of the human head (see Fig. 2). The scalp was assumed to be in direct contact with the air (hair not considered in this study). The SU was placed on the exterior aspect of the skull to emulate partial-thickness implantation (similar to the RNS system [4]). The remaining layers included the subarachnoid space, assumed to primarily contain cerebrospinal fluid (CSF), and the brain. We did not explicitly model the dura and pia mater in this study. The thickness of each tissue layer was taken from the literature, and the specific values are given in Table I.

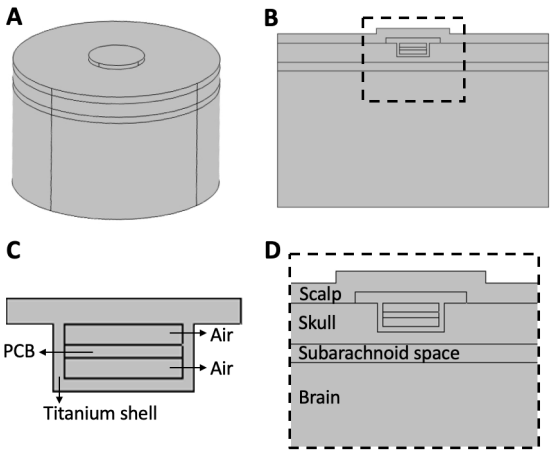

Fig. 2. Different views of the geometric model. (A) 3D view. (B) Central cross-section of the cylinder in (A). (C) The details of the SU. (D) A zoomed-in view of the inset in (B) with relevant tissue layers annotated.

TABLE I
THE THICKNESS OF TISSUE LAYERS AND SU COMPONENTS.

Tissue layer	Thickness (mm)	Reference	SU	Thickness (mm)
Scalp	3.5	[13]	Ti shell	1
Skull	7	[14]	Ti flange	2
Brain	50	[11]	PCB	1
Subarachnoid space	3.2	[15], [16] [17]	Air gaps	1.5

The SU was modeled as a cylindrical, titanium (Ti) shell, with a radius of 6 mm, which contained a printed circuit board (PCB) surrounded by air gaps on both sides. The top of the SU was reinforced with an extra thick 10-mm-radius flange to accommodate its mounting to the bone. The remaining SU dimensions are given in Table I.

B. Mathematical Model

The bio-heat transfer was modeled using Pennes' equation:

$$\rho C \frac{\partial T}{\partial t} = k\nabla^2 T - \rho_\mathrm{b} C_\mathrm{b} \omega (T - T_\mathrm{b}) + Q_\mathrm{m} + Q_\mathrm{ext} \quad (1)$$

where ρ (kg/m^3) and C (J/(kg K)) are the tissue's mass density and specific heat capacity, respectively, and T (K) is the temperature at a position (x, y, z) and time t. The first term on the right-hand side is the heat conduction, where k (W/(m K)) is the tissue's thermal conductivity. The second term models the effect of blood perfusion, where ω ((ml/s)/ml) is the volumetric flow rate of the perfusing blood per unit volume and the subscript, b, refers to arterial blood. Finally, the term Q_m (W/m^3) is the metabolic heat produced by the tissue and Q_ext (W/m^3) is the heat produced by external sources (e.g., the SU in our model). COMSOL applies equation (1) for each tissue layer and SU component, with extraneous terms set to 0 and temperature continuity enforced at the layer interface. The parameter values for each tissue layer are given in Table II, and the thermal conductivities of PCB, titanium, and air are 0.343 [18], 19 [19], and 0.03 [20] (W/(m K)), respectively.

TABLE II
THE THERMAL PROPERTIES OF THE HEAD TISSUES.

Tissue layer	k (W/(m K))	$\rho_\mathrm{b} C_\mathrm{b} \omega$ (W/(m^3 K))	Q_m (W/m^3)	Reference
Scalp	0.342	8954.9	1100	[11]
Skull	0.650	4029.7	26	[11]
Brain	0.528	39483	10383	[11]
Subarachnoid space (CSF)	0.570	-	-	[21]

To estimate the average, long-term thermal impact of the SU, we pursued the steady-state solutions ($\partial T/\partial t = 0$) of (1). To solve this boundary value problem, we applied the following boundary conditions. For the scalp-air interface, we assumed that the heat transfer occurred through free convection with the coefficient $h = 5$ [11]. For the bottom boundary, we assumed the temperature to be equal to the brain core temperature. Finally, we assumed that the lateral boundary was thermally insulated with no radial heat transfer. The last two assumptions are justified given the distance between these boundaries and the SU heat source.

According to ISO 14708-3, active long-term implantable devices should not heat the surrounding tissues beyond 39°C. On the other hand, the brain core temperature tends to be 0.5°C higher than the body core temperature [22] (assumed to be 37°C). Based on these, we conservatively defined the power consumption to be safe if it caused a rise in the surrounding tissue temperature of $\leq$1°C.

We first simulated the effect of the SU with no power consumption (referred to as an inactive case) by setting

$Q_{\text{ext}} = 0$ and storing the temperature distribution across the geometric domain described in Section II-A. We then repeated this procedure by assuming a certain level of power consumption, where Q_{ext} was calculated by dividing the power by the volume of the PCB. From this temperature distribution, we then subtracted that of the inactive case and compared this change, ΔT, to the safety threshold of 1°C. We then iterated Q_{ext} and estimated the power budget as the highest value of Q_{ext} that satisfies $\Delta T \leq 1$°C.

III. RESULTS

The boundary value problem was solved using the FEM with COMSOL's adaptive physics-controlled mesh algorithm. To determine the optimal resolution, we repeated simulations by sweeping the element size from coarse to extra fine. The difference in the results produced by a fine and extra fine mesh was negligible, indicating that convergence had been attained. We ultimately chose the extra fine mesh because the simulations were still relatively fast to run.

We ran simulations with the geometric parameters shown in Table I. The implant dimensions were taken from our existing drafts of the SU. While relatively small, this SU is sufficiently large to house our custom ULP front-ends [6], [7]. The thermal properties of the head tissues were taken from Table II. We omitted the perfusion and metabolic heat terms from the subarachnoid layer since it mostly contained CSF. We chose the thermal properties of the SU components as explained in Section II-B. We assumed the blood temperature to be equal to the body core temperature, i.e., $T_{\text{b}} = 37$°C, and the air temperature was set to 24°C [11].

As explained in Section II-B, we simulated the temperature distribution of the inactive case ($Q_{\text{ext}} = 0$), followed by several progressively increasing values of $Q_{\text{ext}} > 0$. For each power consumption level, we then calculated the temperature increase with respect to the inactive case. Due to the radial symmetry of the geometric model (Fig. 2), the results can be summarized by considering the temperature increase along the central axis of the cylinder (worst case scenario). This results in a convenient 1D representation of the temperature increase. Fig. 3 shows the predicted temperature increase along this line for the SU power consumptions ranging from 40 mW to 90 mW. As can be seen, the highest temperature increase is observed near the center of the SU implant, specifically over the line segment corresponding to the PCB. However, ΔT is significantly reduced by the presence of air gaps. As for tissues, the highest ΔT was observed in the skull immediately beneath the SU. For the 75 mW power consumption, no tissue layer experienced $\Delta T > 1$°C, suggesting that this power consumption is still safe for a long-term SU implantation. Conversely, at 90 mW, both the skull and scalp exhibited ΔT above the safety threshold.

Fig. 4 shows the predicted temperature distribution map in response to the 75 mW power consumption. Consistent with Fig. 3, we see the highest overall temperatures in the PCB layer and the highest tissue temperatures at the skull-SU interface. Not surprisingly, we see lower temperatures at the scalp-air interface, especially when moving radially away from the SU.

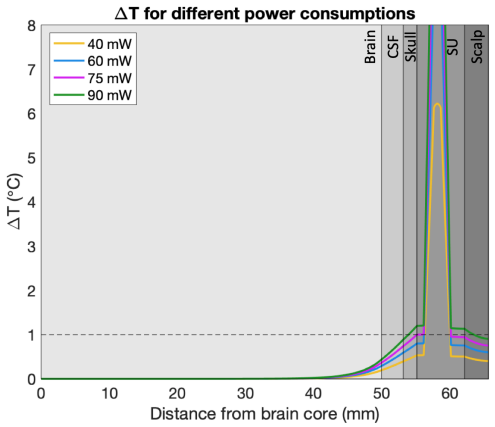

Fig. 3. Temperature increase, ΔT, with respect to the inactive case, calculated along the central axis of the cylinder (Fig. 2). This represents the line with the highest thermal impact of the SU regardless of the power consumption. The vertical lines mark the boundaries of each layer. The dashed horizontal line marks the 1°C safety threshold. We limit $\Delta T \leq 8°C$ for a more detailed view of the temperature increase in the tissue layers.

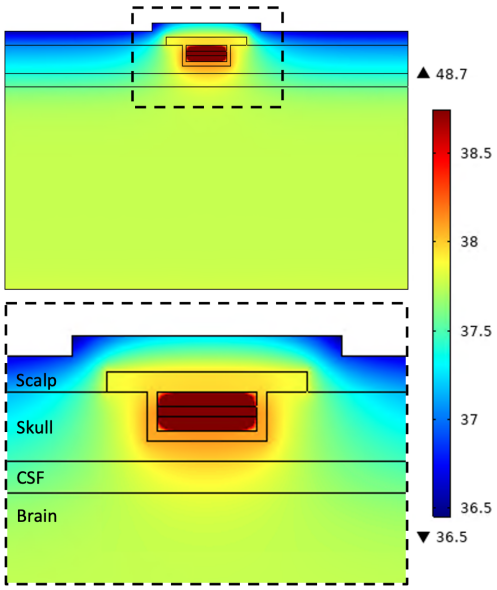

Fig. 4. Temperature distribution (°C) in response to a 75 mW SU power consumption. (Top) The map corresponds to a 2D cross-section passing through the center of the cylinder (Fig. 2). For a more detailed view, the color scale is limited from 36.5 to 39 °C, $T \geq 39°$ C is shown in dark red. (Bottom) The zoom-in of the inset from the top figure.

IV. DISCUSSION AND CONCLUSIONS

By solving the bio-heat equation with physiologically and anatomically constrained parameters, we predicted a maximum power consumption of the SU implant to be 75 mW. This power budget by far exceeds the power consumption of our ULP analog front-end prototypes [5], [6], [7]. Thus, this SU design can sustain the basic functions of the SU such as amplification and serialization. Our current efforts are

directed at endowing the SU with additional elements such as A/D converter and a switched fabric network for delivering cortical stimulation in a fully customized fashion. While the exact power consumption of these elements is not known, the power budget of 75 mW appears abundantly sufficient to sustain these additional functions. In addition to the power consumption, factors such as the SU size and shape, as well as the thickness of the Ti shell and other layers, affect the temperature distribution. Therefore, our finite element model can be used to further optimize these parameters subject to the thermal and surgical safety constraints.

Our simulator represents a simplified model of the bio-heat transfer process. For example, it does not include tissue layers such as the dura and pia mater, and these could be added in the future iterations of the model. Further modifications include the addition of radiative heat transfer at the scalp-air interface, modeling the effect of the hair, and incorporating the brain and skull curvature. However, these modifications have a relatively minor impact and are not expected to significantly change our results. Also, the temperature increase may be more appropriately defined by comparing the simulated temperatures to those of a no-implant case, as opposed to the inactive case as done in this study. Since an inactive SU has a relatively small effect on the temperature distribution of the nearby tissues, we do not expect these results to be fundamentally different from those reported in this study. Finally, long-term heating of tissues can trigger adaptation mechanisms including angiogenesis [23], which, in turn, can significantly alter the effect of blood perfusion. However, this process is incompletely understood and cannot be easily incorporated into the model.

Our short-term goal is to further refine this model and quantify the impact of the above-mentioned factors. More importantly, we will also study the thermal impact of the SU in the BD-BCI context. Namely, delivering cortical stimulation through ECoG electrodes in the vicinity of the SU (Fig. 1) may cause heat, thus altering the temperature distribution of the SU and nearby tissues. We will examine how the two heating sources interact with each other and determine if the power budget of the SU must be adjusted accordingly. Our long-term goal is to test the thermal safety of the SU by implanting it chronically in a large animal model. These *in vivo* studies may ultimately validate our *in silico* predictions, including those made in this study. They will also help us address the effects of long-term active device implantation such as angiogenesis, toxicity, and other factors. Finally, we will also consider other potential direct current leakages between the CWU and the SU.

REFERENCES

[1] E. Kiyatkin. Brain Hyperthermia During Physiological and Pathological Conditions: Causes, Mechanisms, and Functional Implications. *Current Neurovascular Research*, 1(1):77–90, 2005.

[2] T. Lenarz. Cochlear Implant – State of the Art. *Laryngo- rhino-otologie*, 96(S 01):S123–S151, 2017.

[3] A. M. Lozano, N. Lipsman, H. Bergman, P. Brown, S. Chabardes, J. W. Chang, K. Matthews, C. C. McIntyre, T. E. Schlaepfer, M. Schulder, Y. Temel, J. Volkmann, and J. K. Krauss. Deep brain stimulation: current challenges and future directions. *Nature Reviews Neurology*, 15(3):148–160, 2019.

[4] A. Hartshorn and B. Jobst. Responsive brain stimulation in epilepsy. *Ther. Adv. Chronic Dis.*, 9(7):135–142, 2018.

[5] A. Mahajan, A. K. Bidhendi, P. T. Wang, C. M. McCrimmon, C. Y. Liu, Z. Nenadic, A. H. Do, and P. Heydari. A 64-channel ultra-low power bioelectric signal acquisition system for brain-computer interface. In *2015 IEEE Biomedical Circuits and Systems Conference (BioCAS)*, pages 1–4. IEEE, 2015.

[6] A. Karimi-Bidhendi, O. Malekzadeh-Arasteh, M.-C. Lee, C. M. McCrimmon, P. T. Wang, A. Mahajan, C. Y. Liu, Z. Nenadic, A. H. Do, and P. Heydari. CMOS ultralow power brain signal acquisition front-ends: design and human testing. *IEEE T. Biomed. Circ. S.*, 11(5):1111–1122, 2017.

[7] O. Malekzadeh-Arasteh, H. Pu, J. Lim, C. Y. Liu, A. H. Do, Z. Nenadic, and P. Heydari. An Energy-Efficient CMOS Dual-Mode Array Architecture for High-Density ECoG-Based Brain-Machine Interfaces. *IEEE Transactions on Biomedical Circuits and Systems*, 14(2):332–342, apr 2020.

[8] A. Lee, M.-C.and Karimi-Bidhendi, O. Malekzadeh-Arasteh, P. T. Wang, A. H. Do, Z. Nenadic, and P. Heydari. A CMOS MedRadio transceiver with supply-modulated power saving technique for an implantable brain–machine interface system. *IEEE J. Solid-St. Circ.*, 54(6):1541–1552, 2019.

[9] P. T. Wang, E. Camacho, M. Wang, Y. Li, S. J. Shaw, M. Armacost, H. Gong, D. Kramer, B. Lee, R. A. Andersen, et al. A benchtop system to assess the feasibility of a fully independent and implantable brain-machine interface. *J. Neural Eng.*, 16(6):066043, 2019.

[10] M. M. Elwassif, Q. Kong, M. Vazquez, and M. Bikson. Bio-heat transfer model of deep brain stimulation-induced temperature changes. *J. Neural Eng.*, 3(4):306–315, 2006.

[11] S. Kim, P. Tathireddy, R. A. Normann, and F. Solzbacher. Thermal Impact of an Active 3-D Microelectrode Array Implanted in the Brain. *IEEE T. Neur. Sys. Reh.*, 15(4):493–501, 2007.

[12] P. D. Wolf. Chapter 3 Thermal Considerations for the Design of an Implanted Cortical Brain – Machine Interface (BMI). pages 1–20, 2019.

[13] H. Hori, G. Moretti, A. Rebora, and F. Crovato. The thickness of human scalp: normal and bald. *The Journal of investigative dermatology*, 58(6):396–399, 1972.

[14] H. A.M. Mahinda and O. P. Murty. Variability in thickness of human skull bones and sternum - An autopsy experience. *Journal of Forensic Medicine and Toxicology*, 26(2):26–31, 2009.

[15] B. Neil Cuffin and D. Cohen. Comparison of the magnetoencephalogram and electroencephalogram. *Electroencephalography and Clinical Neurophysiology*, 47(2):132–146, 1979.

[16] P. Berg and M. Scherg. A fast method for forward computation of multiple-shell spherical head models. *Electroen. Clin. Neuro.*, 90(1):58–64, 1994.

[17] F. B. Haeussinger, S. Heinzel, T. Hahn, M. Schecklmann, A. C. Ehlis, and A. J. Fallgatter. Simulation of near-infrared light absorption considering individual head and prefrontal cortex anatomy: Implications for optical neuroimaging. *PLoS ONE*, 6(10), 2011.

[18] F. Sarvar, N. J. Poole, and P. A. Witting. PCB glass-fibre laminates: Thermal conductivity measurements and their effect on simulation. *Journal of Electronic Materials*, 19(12):1345–1350, dec 1990.

[19] R.W. Powell and R.P. Tye. The thermal and electrical conductivity of titanium and its alloys. *Journal of the Less-Common Metals*, 3(3):226–233, 1961.

[20] S. G.S. Beirão, A. P.C. Ribeiro, M. J.V. Lourenço, F. J.V. Santos, and C. A. Nieto De Castro. Thermal conductivity of humid air. *International Journal of Thermophysics*, 33(8-9):1686–1703, 2012.

[21] P. A. Hasgall, F. Di Gennaro, C. Baumgartner, E. Neufeld, B. Lloyd, M. C. Gosselin, D. Payne, A. Klingenböck., and N. Kuster. IT'IS Database for thermal and electromagnetic parameters of biological tissues. 2018.

[22] H. Wang, B. Wang, K. P. Normoyle, K. Jackson, K. Spitler, M. Sharrock, C. M. Miller, C. Best, D. Llano, and R. Du. Brain temperature and its fundamental properties: A review for clinical neuroscientists. *Front. Neurosci.*, 8:307, 2014.

[23] C. R. Davies, F. Fukumura, K. Fukamachi, K. Muramoto, S. C. Himley, A. Massiello, J.-F. Chen, and H. Harasaki. Adaptation of Tissue to a Chronic Heat Load. *ASAIO Journal*, 40(3):M514–M517, 1994.